A R C H I V E S O F M E T A L L U R G Y A N D M A T E R I A L S
Volume 54 2009 Issue 2

W. KAPTURKIEWICZ*, E. FRAŚ*, A. A. BURBELKO*

MODELING THE KINETICS OF SOLIDIFICATION OF CAST IRON WITH LAMELLAR GRAPHITE

MODELOWANIE KINETYKI KRYSTALIZACJI ŻELIWA Z GRAFITEM PŁATKOWYM

The most important results of own studies on modeling the solidification kinetics in lamellar (flake) graphite cast iron were reviewed. A set of basic equations used for modeling the solidification process in macro- and micro-scales was given. A numerical solution of these model equations enables the determination of thermodynamic equilibrium temperature and actual temperature of cast iron solidification, the cooling rate, the heat flux generated during solidification, the fractions of the solidified structural constituents, the size of graphite eutectic grains and austenite dendrites, thickness of graphite lamellar, as well as the segregation of cast iron alloying constituents in liquid phase and in the forming grains. It has also been proved and confirmed by experiments that the grains of graphite eutectic are formed in a two-step process, that is, at the beginning and end of the solidification process. Some important differences in the size of graphite precipitates were observed to exist between the cast plate and cylinder.

Zaprezentowano najistotniejsze rezultaty własnych prac, dotyczących modelowania komputerowego krystalizacji żeliwa z grafitem płatkowym. Przedstawiono zestaw podstawowych równań procesu, odnoszących się do mikro i makro skali. Rozwiązanie numeryczne zestawu równań w postaci programu symulacyjnego pozwoliło na wyznaczenie przebiegu temperatury w czasie stygnięcia odlewu wraz z rozkładem temperatury równowagowej, ciepła generowanego podczas krystalizacji, ilości frakcji zakrzepłej poszczególnych składników strukturalnych żeliwa, wymiaru ziaren austenitu i eutektyki grafitowej, wymiary płatków grafitu jak również mikrosegregacji składników stopu w ziarnach. Potwierdzono eksperymentalnie, że ziarna eutektyki grafitowej mogą zarodkować w dwóch etapach: na początku i pod koniec procesu krystalizacji. Istotne różnice zauważono w wymiarach grafitu w zależności od kształtu odlewu.

Introduction

Cast iron with flake graphite (Fig. 1) is the most important and most often used in practice cast alloy. Simultaneous grains nucleation and growth as well as the development of the local thermal gradients within the melt make difficult to discern the role of all the factors involved in cast iron solidification. Hence, the nature of the events that take place during solidification is rather complex, and computer modeling can help to close the existing gap between the analytical and empirical understanding of casting solidification. The literature on numerical modeling is very comprehensive (mainly proceedings of the conference on Modeling of Casting, Welding and Advanced Solidification Processes) and its synthetic review has been given by Stefanescu [1, 2] and Rappaz [3]. The aim of the present work is to relate the results of own investigation [4 - 7] confined to the cast iron with flake graphite.

* AGH UNIVERSITY OF SCIENCE AND TECHNOLOGY, 30-059 KRAKOW, 23 REYMONTA STR., POLAND

a)

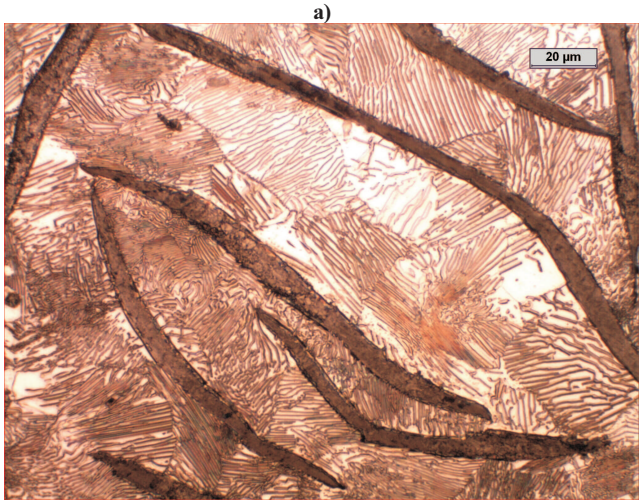

b)

Fig. 1. Microstructure of lamellar graphite in cast iron: a) non-etched, b) etched (Nital)

1. Process model

The model of the process has been based on the following assumptions:

- a casting of plate or cylinder (1D) made from hypoeutectic Fe-C-Si-P alloy is solidifying in sand mould from pouring temperature to a eutectoid point;
- the change of thermodynamic conditions caused by the change of temperature is proceeding according to an Fe-C system allowing for the effect of Si and P;
- a non-equilibrium model of the nucleation and growth of the austenite and graphite eutectic grains;
- the changes of thermodynamic conditions result in the formation of carbon concentration gradients, where mass diffusion due to the presence of these gradients acts as a driving force for the austenite-graphite phase boundary movement;
- a 1D concentration system with planar austenite-graphite phase boundary has been adopted.

1.1. A set of basic equations

The model combines a macro model (heat transfer) with micro model (nucleation and growth of grains).

Heat transfer

The macro temperature field in casting-mold system is:

$$\frac{\partial T}{\partial \tau} = a\nabla^2 T + \frac{q_s}{c_v}, \tag{1}$$

where T,τ – temperature and time, a – thermal diffusivity (for metal or for mold), q_s – heat generation rate of phase transformations, c_v – volumetric specific heat.

Volume fraction

In order to calculate the true volume fraction of solid, one must include the effect of grain impingement. The true volume fraction of solid V_S can be described by Kolmogorov equation [8]:

$$f_s = 1 - e^{-\Omega}, \quad (2)$$

where Ω – so-called "extended" volume of all solid grains. According to Kolmogorov [8]:

$$\Omega = -\frac{4\pi}{3} b \int_0^t \alpha(t') \left(\int_{t'}^t u(\tau)\, d\tau \right)^3 dt', \quad (3)$$

where t' – nucleation time, α(t') – rate of the grain nucleation, u(τ) – linear velocity of the growth, $\int_{t'}^{t} u(\tau)\, d\tau$ – grain radius, b – shape coefficient (e.g. b = 1 for globular grains and b = 0.3 for dendrite grains).

Nucleation

It is well known that liquid cast iron contains undissolved particles of various sizes. Hence, upon alloy undercooling beyond a critical value, these particles exceed the minimum sizes needed for stable growth. Hence, growing nuclei are continually developed until the time when the metal attains its maximum level of undercooling. Afterward, with the progress of recalescence, no new nuclei form because all the particles larger then the critical size (which corresponds to maximum undercooling) were already exhausted. Activation of smaller particle substrates as active nuclei will require undercooling, which will have to exceed the maximum value. A comparison of these observations with the typical pattern of a cooling curve obtained from the central part of a eutectic or nearly-eutectic iron casting (Fig. 2) indicates that, at the time B, corresponding to the maximum undercooling ΔT^{I}_{max} primary nucleation ends. Between B and C, grain growth occurs without further nucleation, and can only take place whenever the ΔT^{I}_{max} is exceeded (between points C and D). According to Fig. 2, a second maximum in the undercooling develops between C and E (ΔT^{TI}_{Imax} at D), where E marks the end of solidification.

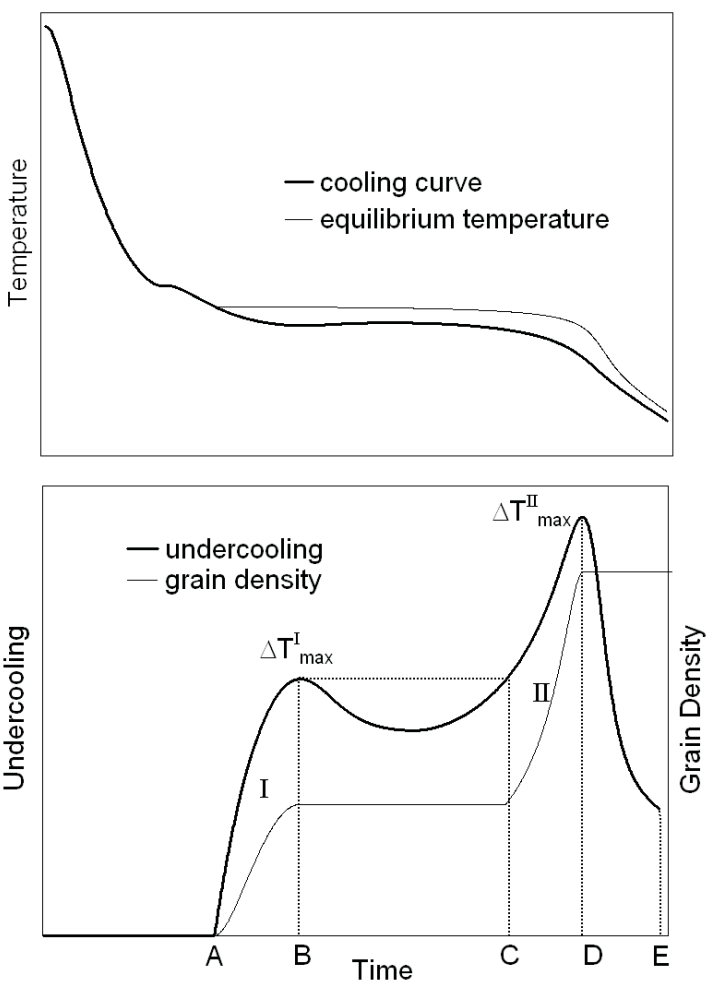

Fig. 2. Cooling curves end equilibrium temperatures for stable graphite eutectic, undercooling and number of grain nucleated in the central part of cylindrical casting (schematic) [5]

To compute the density of the formed Ni nuclei the following relationship has been adopted [9]:

$$N_i = \psi_i(\Delta T_i)^{\beta_i}, \quad (4)$$

where ΔT_i is undercooling and ψ_i, β_i are the nucleation coefficients of "i" solidifying component.

Growth of grains

The dendritic radius of austenite grains has been determined basing on equations given in [10]. Rate of growth for eutectic grains:

$$u_e = \mu \cdot \Delta T^2, \quad (5)$$

where Δ T – degree of undercooling, μ – eutectic growth coefficient.

Growth of graphite

The description below relates to a model of the graphite growth in austenite since the onset of crystallisation process. The concentration field has been schematically drawn in Figure. 3a and compared with the phase equilibrium diagram in Figure 3b.

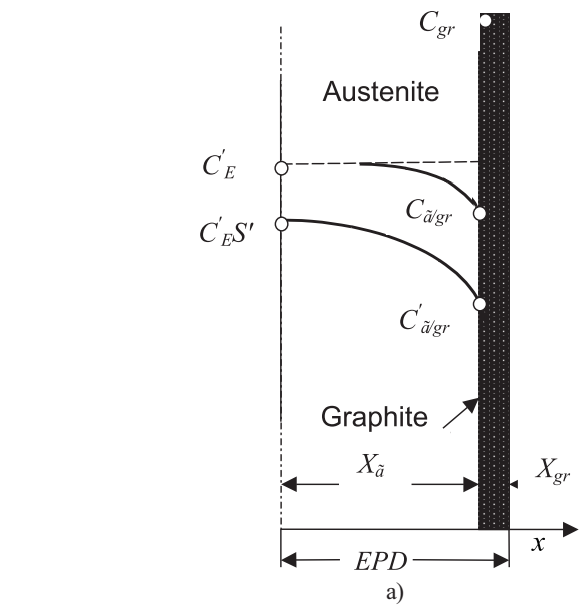

a)

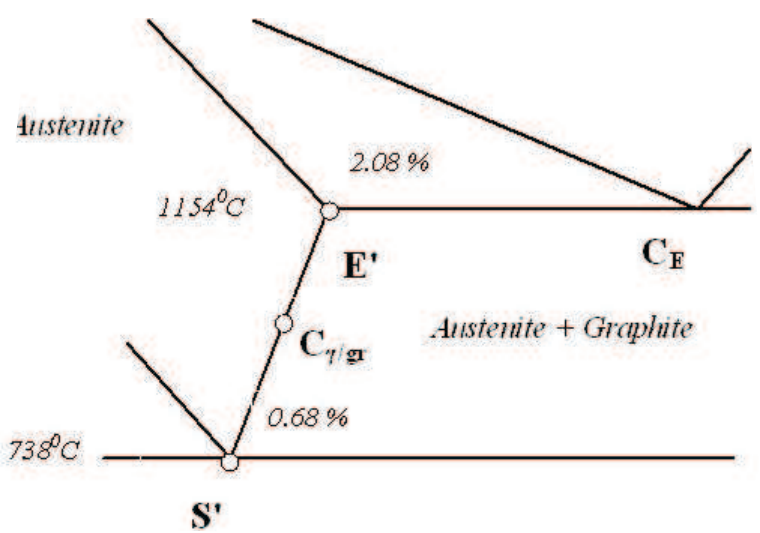

b)

Fig. 3. Schematic distribution of concentration values in austenite-graphite system (a) as compared with phase equilibrium diagram (b)

The concentration field in an austenite-graphite system is described by the following equation:

$$\frac{dC}{d\tau} = \frac{\partial C}{\partial x}\left(\frac{dx}{d\tau}\right) + \frac{\partial C}{\partial \tau}, \tag{6}$$

where – $\partial C/\partial\tau$ from Fick's equation for the stationary phase boundary – we have:

$$\frac{\partial C}{\partial \tau} = D\frac{\partial^2 C}{\partial x^2}, \tag{7}$$

where: D – is the diffusion coefficient of carbon in austenite.

A member of the substantial derivative $dx/d\tau$ is the velocity of the phase boundary movement u, which can be computed from balance equation (Fig. 3):

$$\frac{u}{C_{\gamma/gr} - C_{gr}} = -D\left(\frac{\partial C}{\partial x}\right)_{\xi-}, \tag{8}$$

where: ξ – the austenite-graphite phase boundary

The above system of equations was solved by the finite difference method using the procedure of a moving network described in [11].

Equilibrium temperature and segregation

The equilibrium temperatures T_γ for solidifying austenite and T_e for eutectics can be represented by linear functions of carbon, silicon and phosphorus concentration in liquid cast iron [12, 13].

According to Kobayashi [14] the solute concentration in the solidifying phases is strongly influenced by the magnitude of the diffusion coefficients. Hence, for solute of relatively high diffusivity (e.g. carbon in austenite), the solute concentration in the liquid phase can be approximated by the mass balance. Alternatively, the Scheil equation can be used in dealing with low diffusivity solutes, such as in the case of silicon or phosphorus in austenite.

2. Results and discussion

2.1. Cooling curves, cooling rates and volumetric heat fluxes

Figures 4 and 5 show graphically the model predictions for cast iron of eutectic and hypoeutectic composition (plate casting; thickness 2 cm). Notice from these figures the influence exerted by the relative locations within the melt on the cooling curves, cooling rates and volumetric heat fluxes generated. Here, "c" refers to the center of the casting, whereas "s" indicates surface of the casting.

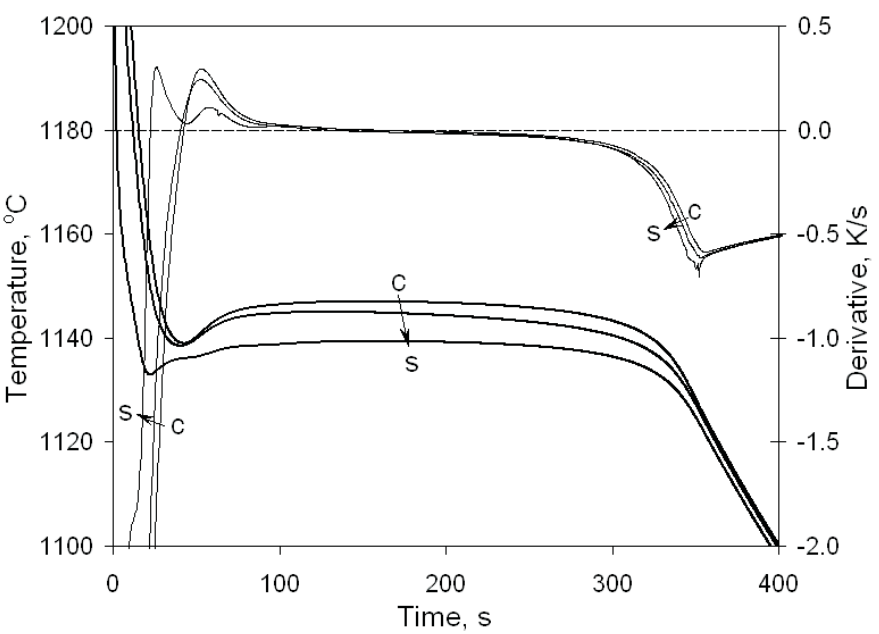

Fig. 4. Solidification kinetics of a cast iron of eutectic composition (Fe-4.26 wt. % C), "c" refers to the center and "s" refers to the surface of the casting [6]

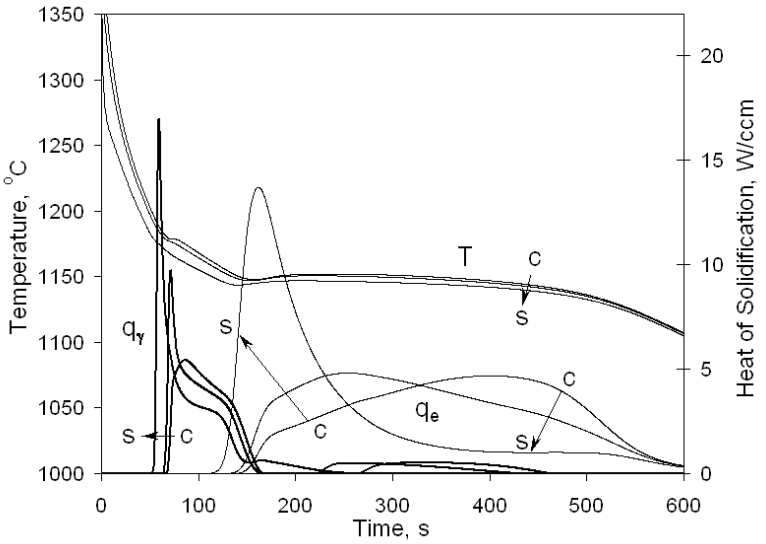

Fig. 5. Solidification kinetics of hypoeutectic cast iron of 3.5 wt. % C, "c" and "s" – as above [6]

It is worth noting that the solidification of austenite dendrites also occurs during the eutectic transformation, but thermal effects of the dendritic solidification during this transformation are quite insignificant (Fig. 5).

Figure 6 shows the cooling curves at two points within the cylindrical casting of 3-cm diameter. Notice that the experimental data and computer modeling are agrees with each other and there are only minor variations.

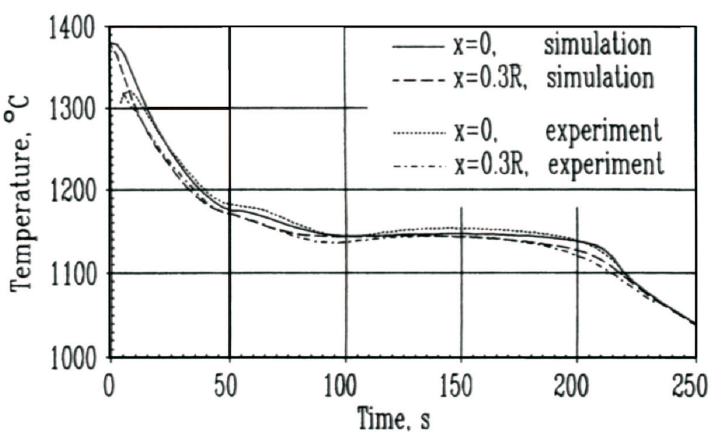

Fig. 6. A comparison between experimental and predicted cooling curves at two locations inside cylindrical casting [6]

The castings of plate and cylinder are characterised by the same modulus X_1 = 1.0 cm which, according to numerous studies, should yield similar solidification conditions.

The following parameters were adopted in computations:

- Casting: plate 2 cm thick and cylinder of 4 cm diameter; sand mould of 10 cm wall thickness.
- Cast metal: 3.0%C, 2.0%Si, 0.0075%P (mass %): λ = 0.37 W/cm K; c = 0.753 J/g K; ρ = 7.2 g/cm^3
- The heat of austenite and eutectic solidification: L_γ = 2028 J/g; L_e = 1952.4 J/g
- Nucleation parameters:
  - for austenite: $\mu_\gamma = 3.14\text{x}10^{-6}$ cm/s K; ψ_γ = 200 cm^{-3}K^{-2}
  - for graphite eutectic: $\mu_\gamma = 5.0\text{x}10^{-6}$ cm/s K; ψ_γ = 3.5 cm^{-3}K^{-2}
- The coefficient of carbon diffusion in austenite: D = $1\text{x}10^{-6}$ cm^2/s
- Mould material: λ = 0.0103 W/cm K; c = 1.09 J/g K; ρ = 1.73 g/cm^3.

Yet, a rough comparison of the temperature fields (Figure 7) indicates an obvious difference in the run of the cooling curves. The difference is particularly visible in Figure 8, which covers the whole solidification range, including location of the point of maximum undercooling and the shape of recalescence. Very characteristic is the difference in time and temperature at an instant when the solidification process has been completed. It is due to the effect of casting configuration and microsegregation of the alloying elements (silicon, phosphorus and carbon).

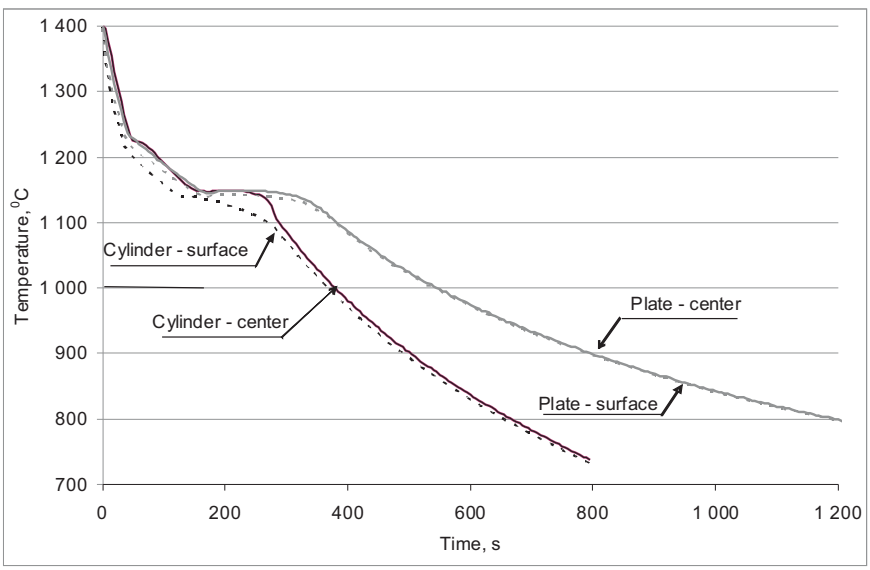

Fig. 7. Temperature curves for the cast plate and cylinder (modelling)

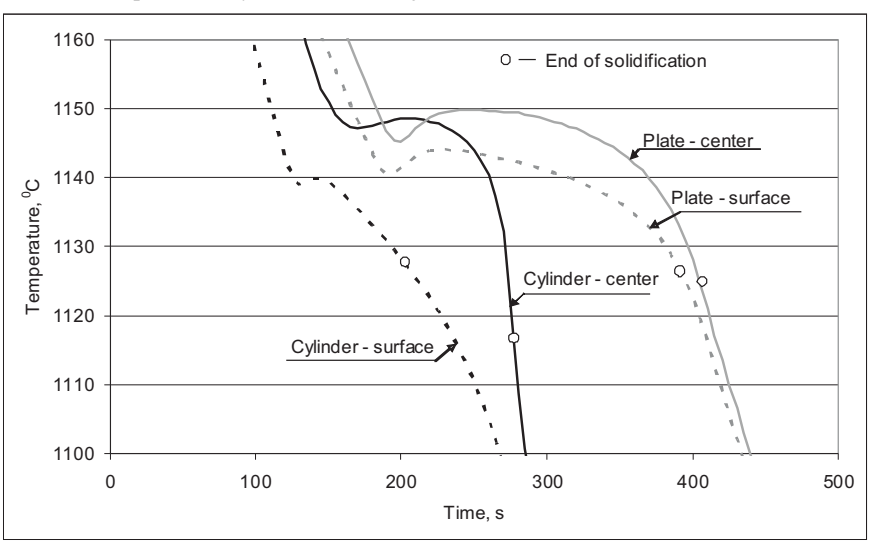

Fig. 8. Temperature curves for the solidification range of cast plate and cylinder (a fragment of Fig. 3). Points mark the end of solidification in the middle of the casting and near its edge

The differences in casting configuration cause differences in the nucleation kinetics and final grain density (Fig. 9). The differences in grain density between the casting surface and its centre are much smaller in the cast plate than they are in the cast cylinder (in computations the possibility of a secondary nucleation has been neglected).

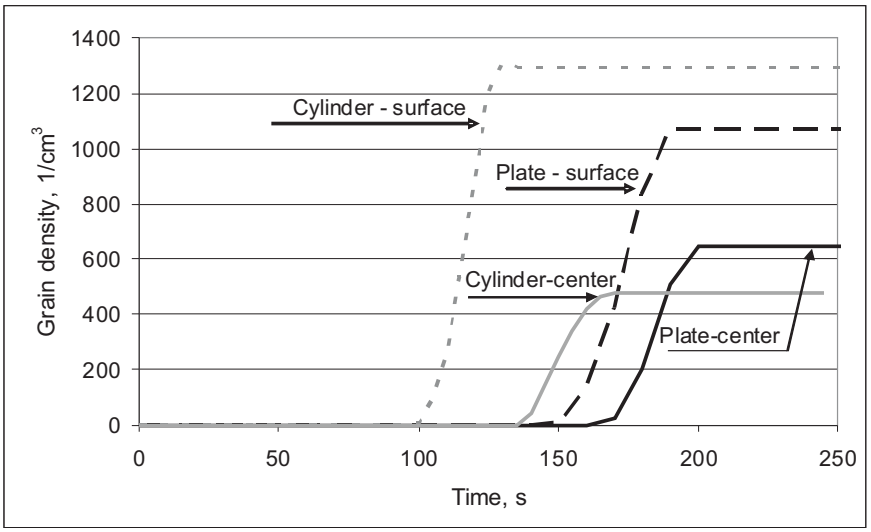

Fig. 9. The kinetics of nucleation of graphite eutectic grains in the cast plate and cylinder

From Figure 10 it follows that there are some important differences between the cast plate and cylinder as regards the thickness of graphite precipitates. On the other hand, under the same cooling conditions, the difference between the casting surface and its centre is negligible for both the plate and cylinder casting.

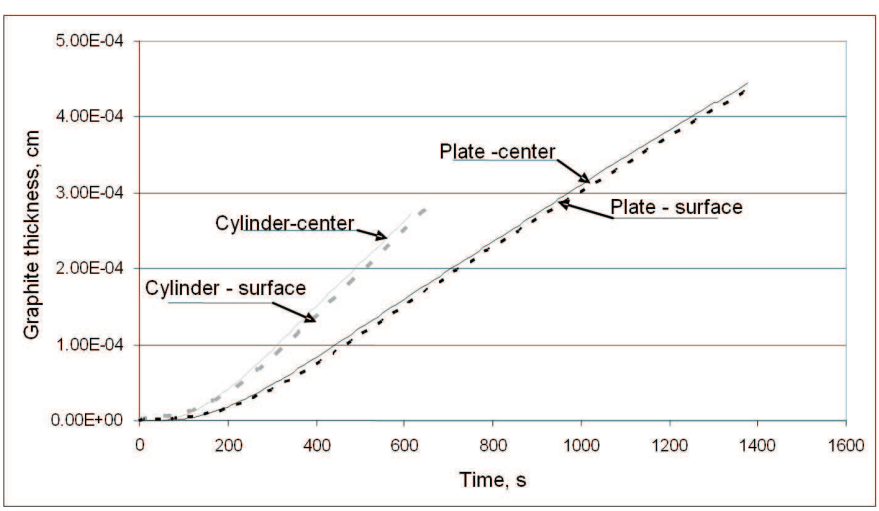

Fig. 10. The kinetics of graphite thickness growth in the cast plate and cylinder

2.2. Eutectic structure

The experimental results confirm the presence of a fine graphite eutectic grain region in the central zone of the casting, which can be identified as a secondary nucleation zone (Fig. 11).

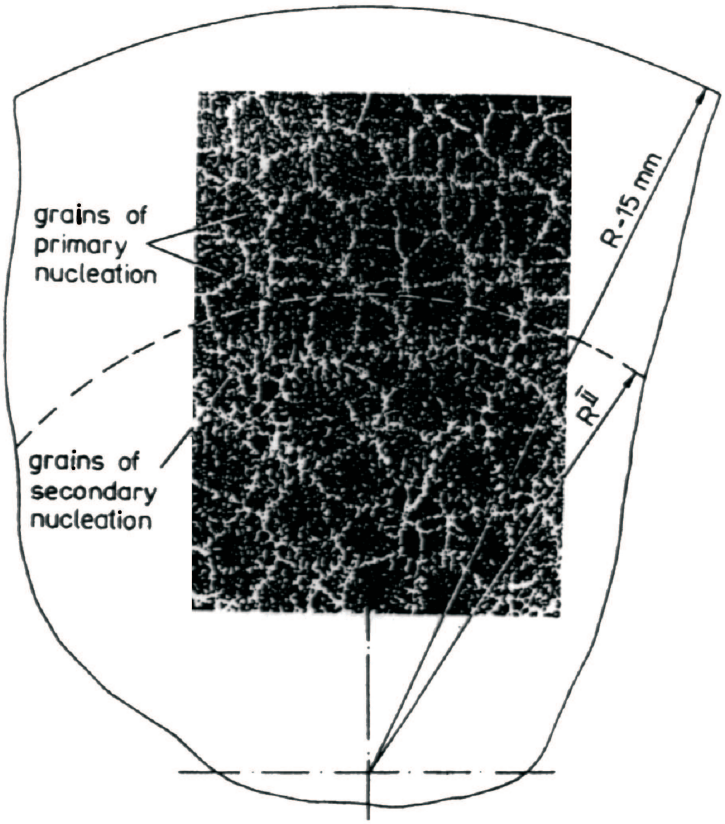

Fig. 11. Schematic representation of casting macrostructure cross section. RII represents the computed range of occurrence of secondary nucleation [7]

Figure 12 shows the predicted pattern of undercooling with respect to the eutectic equilibrium temperature at five locations within the cross section of the casting. Moreover, this figure can be correlated with Fig. 2 for similar solidification times. Accordingly, the proposed model agrees with the expected grain formation mechanism, and the development of a secondary grain nucleation zone. In particular, secondary nucleation is expected to occur in the zone of the casting, where a second undercooling maximum arises that exceeds the first one (see Fig. 2b). From Fig. 12 and 7 it can be observed that this condition is met at solidification distances of 0.1, 0.3 and 0.5R (denoted as R^{II} in Fig. 11) from the main axis.

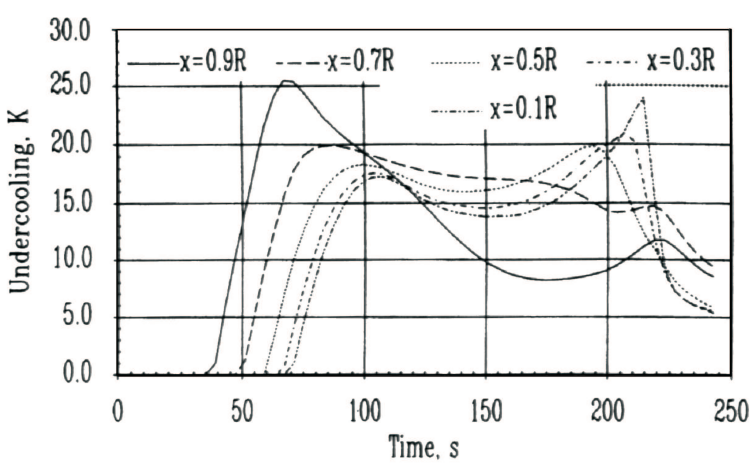

Fig. 12. Undercooling curves predicted at five different locations inside cylindrical casting [7]

The experimental outcome (Fig. 11) indicates that the number of primary nucleation grains increases as the surface of the casting is approached, while secondary nucleation grains are dominant in the central zone of the casting. This agrees with the simulation predictions of maximum secondary undercooling at solidification distances below 0,5 R (Fig. 11). In particular, Fig. 12 shows that the computer simulation predictions (solid and broken lines) very closely follow the experimental outcome.

3. Segregation Effects

The predictions of C, P and Si segregation during the solidification of the hypoeutectic alloys are shown in Fig. 13. In particular, this figure shows that the carbon content in the liquid, near to the surface of solidifying austenite is increasing with time. Furthermore, at a given time, the carbon concentration is essentially the same, regardless of the particular location in the melt. This is explained by the relatively high carbon diffusivity at these temperatures. The carbon concentration in the liquid keeps on increasing until the onset of eutectic solidification. Once this occurs, the carbon concentration in the melt tends to remain constant.

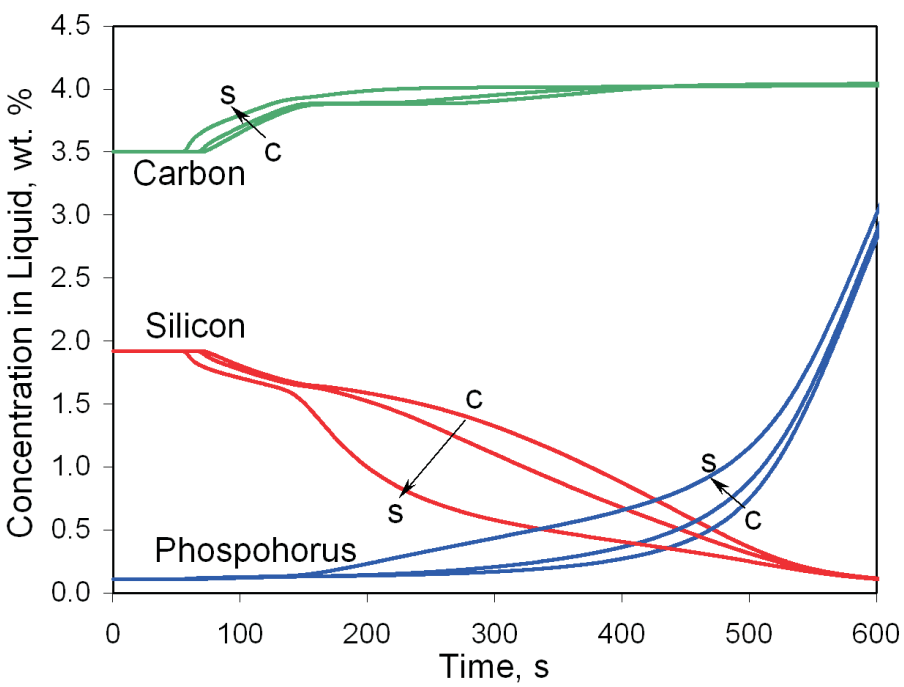

Fig. 13. Predicted evolution of C, Si and P concentration profiles in the liquid melt during the solidification in the 3 points across the casting ("c" refers to the center and "s" refers to the surface of the casting) [6]

Figure 14 shows the model predictions for the distribution of Si and P as a function of the grain radii. According to the model predictions, Si and P exhibit opposite trends (i.e., the liquid surrounding the grains gets depleted in Si and enriched in P). Hence, the model predictions indicate that the redistribution of P and Si is enhanced during the last stages of dendritic or eutectic growth (especially during eutectic grain growth). Furthermore, the predictions of P enrichment and Si depletion in the liquid during the solidification of cast iron agree with the experimental evidence.

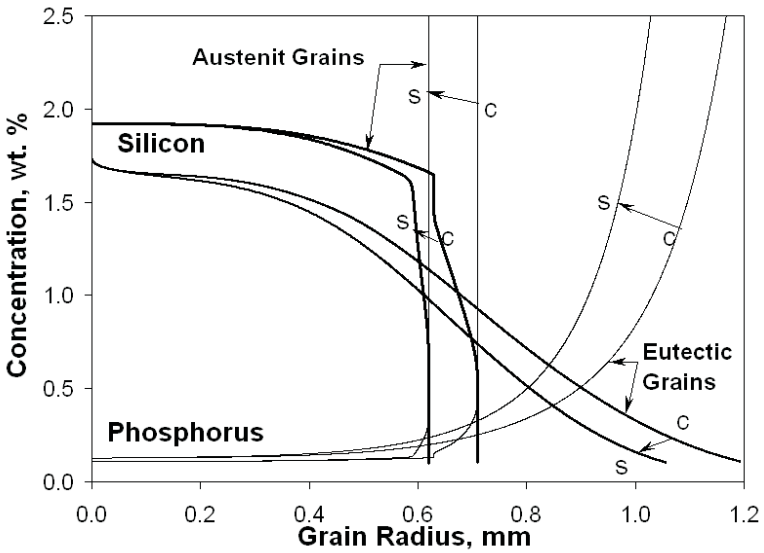

Fig. 14. Concentration profiles and their relationships to the austenitic or eutectic grain radii for P and Si for the center and surface of the casting [6]

4. Conclusions

The results of own studies on modeling the solidification kinetics in lamellar (flake) graphite cast iron were reviewed. A numerical solution of model equations enables the determination of thermodynamic equilibrium temperature and actual temperature of cast iron solidification, the cooling rate, the heat flux generated during solidification as well as the heat volume accumulated in casting, the fractions of the solidified structural constituents, the size of graphite eutectic grains and austenite dendrites, as well as the segregation of cast iron alloying constituents in liquid phase and in the forming grains.

It has also been proved and confirmed by experiments that the grains of graphite eutectic are formed in a two-step process, that is, at the beginning and end of the solidification process.

The results of modelling indicate a significant difference in the solidification kinetics and structure refinement (the density of eutectic grains) between the cast plate and cylinder, both castings being characterised by the same modulus (reduced wall thickness) and solidifying in sand moulds.

Some important differences in the size of graphite precipitates were observed to exist between the cast plate and cylinder, while under the same cooling conditions, the differences between the casting surface and its centre were only negligible for both the plate and cylinder.

Acknowledgements

This work was carried out under MNiSW (Ministry of Science and Higher Education, Warsaw), project No N507 071 31/1623.

REFERENCES

[1] D. M. Stefanescu, Science and Engineering of Casting Solidification. Springer Verlag, Second ed. (2008).

[2] D. M. Stefanescu, Modeling of Cast iron Solidification – The Defining Moments. Metall. Mater. Trans. A, 38A, 1433-1447 (July 2007).

[3] M. Rappaz, M. Bellet, M. Deville, Numerical Modeling in material Science and Engineering, Springer Verlag (2003).

[4] E. Fraś, W. Kapturkiewicz, H. Lopez, Macro and Micro Modeling of the Solidification Kinetics of Cast Iron. AFS Transactions 100, 583-590 (1992).

[5] E. Fraś, W. Kapturkiewicz, A. Burbelko, Computer Modeling of Fine Graphite Eutectic Grain Formation in the Casting Central Part. Proceedings of the VI Conference in a Series on Modeling of Castings and Welding Processes, Palm Coast, Florida, 261-268 (1993).

[6] E. Fraś, W. Kapturkiewicz, A. A. Burbelko, H. Lopez, Numerical Simulation of the Solidification Kinetics of Cast Iron. Int. J. Cast Metals 6, 2, 91-98 (1993).

[7] E. Fraś, W. Kapturkiewicz, A. A. Burbelko, H. Lopez, Secondary Nucleation of Eutectic Graphite Grains. AFS Transactions **96**, 1-4 (1996).

[8] A. N. Kolmogorov, On the Statistical Theory of Metal Solidification (in Russian), Bull. Acad. Sci. USSR **3**, 355-359 (1937).

[9] W. O l d f i e l d, A Quantitative Approach to Casting Solidification: Freezing of Cast Iron. Trans ASM 59, 945-961 (1966).
[10] J. L i p t o n, M. E. G l i c k s m a n, W. K u r z, Dendritic Growth into Undercooled Alloy Melts, Mat. Sci. Eng. **65**, 57-63 (1984).
[11] W. K a p t u r k i e w i c z, E. F r a ś, A. A. B u r b e l k o, Computer Simulation ofAustenitizing Process in Cast Iron with Pearlitic Matrix, Mat. Sc. Eng. **A 413-414**, 352-357 (2005).
[12] R. D ö p p, The Metallurgy of Cast Iron. Georgi Publishing Co, S. Saphorin, p 655 (1975).
[13] F. N e u m a n n, The Influence of Additional Elements on the Physics Chemical Behavior of Carbon in Carbon Saturated Molten Iron, Recent Research in Cast Iron, Gordon and Breach, New York, 659 (1968).
[14] S. K o b a y s h i, Solute Redistribution during Solidification with Diffusion in Solid Phase. A Theoretical Analysis. J. Cryst. Growth **88**, 87-96 (1988).

Received: 10 May 2009.